Journal of Power Sources 266 (2014) 43–50

Contents lists available at ScienceDirect

Journal of Power Sources

journal homepage: www.elsevier.com/locate/jpowsour

Magnetron sputtering amorphous carbon coatings on metallic lithium: Towards promising anodes for lithium secondary batteries

Y.J. Zhang, X.Y. Liu, W.Q. Bai, H. Tang, S.J. Shi, X.L. Wang, C.D. Gu, J.P. Tu*

State Key Laboratory of Silicon Materials, Key Laboratory of Advanced Materials and Applications for Batteries of Zhejiang Province, and Department of Materials Science and Engineering, Zhejiang University, Hangzhou 310027, China

HIGHLIGHTS

- Amorphous carbon coatings were deposited onto the surface of metallic lithium.
- The formation of dendritic can be prevented according to the SEM photograph.
- The electrochemical performance is promoted due to the existence of a-C coating.
- The thickness of a-C coating affects the electrode performance from two aspects.

ARTICLE INFO

Article history:
Received 27 December 2013
Received in revised form
13 April 2014
Accepted 30 April 2014
Available online 14 May 2014

Keywords:
Amorphous carbon
Dendritic formation
Coating thickness
Lithium secondary battery
Magnetron sputtering technique

ABSTRACT

All the Li metal anode-based batteries suffer from a high propensity to form Li dendrites. To prevent the formation of dendritic lithium on the electrodes, amorphous carbon coatings are deposited onto the surface of metallic lithium foil by magnetron sputtering technique. The electrochemical performances of the amorphous carbon-coated lithium (Li/C) electrodes are investigated by galvanostatic charge/discharge tests, cyclic voltammetry (CV) and electrochemical impedance spectroscopy (EIS). The compact carbon coatings on the surface of lithium foil can suppress the growth of dendritic lithium during charge–discharge process. The thickness of amorphous carbon coating affects the electrode from two aspects; the thick coating can prevent the formation of dendritic lithium much efficiently, but lead to a large impedance of Li^+ transfer.

1. Introduction

Rechargeable batteries with high energy density are essential for solving imminent energy and environmental issues [1,2]. In the past decades, a lot of research has been focused on finding new anode materials to improve the lithium storage capability of lithium secondary batteries [3–11]. Metallic Li has an extremely high theoretical specific capacity (3860 mAh g^{-1}), low density (0.59 g cm^{-3}) and the lowest negative electrochemical potential (−3.045 V *vs.* standard hydrogen electrode (SHE)), thus rechargeable Li metal batteries have been called the "Holy Grail" of energy storage systems and have been investigated extensively during the last 40 years. Recently, the lithium–sulfur and lithium–air batteries have attracted attention for their extremely high capacity [12–19]. So as to meet the ever-growing demand for lithium secondary batteries with higher power and energy densities, the improvement in electrochemical performance of Li metal anode is extremely urgent.

In order to achieve the commercialization of Li metal anode, there are two main problems to be solved [20–27]. One is that metallic Li is too active and it easily reacts with electrolyte, which results in a low cycling efficiency. The other one is the formation of dendritic lithium between the interface of Li anode and electrolyte. This kind of morphology may puncture the separator and lead to the safety problem. According to previous reports [28,29], the dendritic formation can be influenced by many kinds of factors, such as lithium surface tension and surface energy. Among them, it is mainly ascribed to the continuous deposition and dissolution of Li^+ during charge/discharge processes. As a result, the electrochemical performance is very poor due to the non-uniformity of solid electrolyte interface (SEI) layer.

Most approaches to dendrite prevention focus on improving the stability and uniformity of the SEI layer by adding some additives,

* Corresponding author. Tel.: +86 571 87952573; fax: +86 571 87952856.
E-mail addresses: tujp@zju.edu.cn, tujplab@zju.edu.cn (J.P. Tu).

http://dx.doi.org/10.1016/j.jpowsour.2014.04.147
0378-7753/

such as HF [30], AlI_3 [31] and carbonate [32,33]. But it is very difficult to achieve sufficient passivation between Li metal anode and the electrolyte, as indicated by Aurbach [23]. The approach to form protective films on the surface of metallic Li before electrochemical process has also been reported. Such protective films must conduct Li ions, and at the same time can prevent the contact between Li and electrolyte. Arie et al. reported that C_{60} [28] and diamond like carbon [34] film deposited by vacuum techniques can play a role as a passive layer against the side reaction between Li surface and electrolyte. In Wu's work [35], a Li_3N film was fabricated on Li surface as a protective layer by the direct reaction between Li and N_2 gas at room temperature. Although the cycling performance of Li_3N modified Li electrode is better than the as-received Li, the preparation method is complicated. Amorphous carbon (a-C) films were usually used as protective coatings in mechanical applications due to their excellent physical and chemical properties [36–43]. In this present work, we fabricated a-C coatings on metallic Li foil by magnetron sputtering technique. The a-C coatings show positive effects on the electrochemical behaviors of Li in a conventional organic electrolyte. What's more, the magnetron sputtering technique is convenient and suitable for industrial production [44–49]. The effects of sputtering time on the electrochemical properties of Li/C anodes were then investigated.

2. Experimental

2.1. Fabrication of a-C coatings

The a-C coatings were deposited on metallic Li foil (200 μm in thickness) and Si (100) wafer substrates by a closed field unbalance magnetron sputtering system (TAJS-700, TENGAO). The coatings deposited on the silicon wafers were only used to characterize their morphology, as it is hard to observe the cross-section morphology of a-C coating on Li foil directly. The Si substrates were ultrasonically washed in acetone for 20 min, in ethanol for 10 min, and then blow-dried by nitrogen. Prior to deposition, the base pressure of the sputtering system was evacuated to 4×10^{-3} Pa, and then argon gas was introduced to keep the working pressure of 0.2 Pa. In order to remove the oxides and adsorptions, the substrates were etched by Ar^+ bombardment at a negative bias of 500 V for 30 min. During the deposition process, the current of graphite targets was kept at 1 A, and the sputtering bias was maintained at 50 V. The a-C coatings were deposited for 20 min, 40 min and 60 min, respectively.

2.2. Characterization

The surface and cross-section morphologies of the a-C coatings were observed using scanning electron microscope (SEM, Hitachi S-4800 equipped with GENENIS 4000 EDAX detector). The bonding structure of coatings was characterized by an X-ray photoelectron spectroscopy (XPS) using an ESCAL 220i-XL electron spectrometer, operating with a monochromated Al-Kα X-ray radiation source in a base pressure of 10^{-7} Pa. To avoid air contamination, the Li electrode samples were transferred in the sealed box filled with argon gas and loaded into the SEM and XPS machine under pure argon atmosphere.

All the electrochemical measurements were performed with sealed CR2025 coin cells. The a-C coated Li foil pressed on copper sheet (0.05 mm in thickness) was used as the working electrode and a copper sheet with a diameter of 15 mm was used as the counter electrode. Before the tests, the copper sheet was cleaned with the diluted hydrochloric acid at first, then washed with alcohol and blow-dried in air. Celgard 2300 was used as the separator and a solution of 1 M $LiPF_6$ in ethylene carbonate (EC) and dimethyl carbonate (DMC) (1:1 in volume) was employed as the electrolyte. The cells were assembled in a glove box filled with high-purity argon. The charge–discharge measurements were carried out on LAND battery test system (Wuhan, China). Li of 0.9 C cm^{-2} was deposited at a cycling current density of 0.5 mA cm^{-2}. The cut-off potential was controlled at 1.0 V (*vs.* Li/Li^+) for the Li dissolution. The Li cycling efficiency (Eff) is calculated using Eq. (1):

$$\mathrm{Eff} = \frac{Q_{\mathrm{dissolution}}}{Q_{\mathrm{deposition}}} \times 100\% \quad (1)$$

where $Q_{\mathrm{depositon}}$ represents the charge quantity of Li deposition, and $Q_{\mathrm{dissolution}}$ represents the dissolution quantity of deposited Li [35].

Cyclic voltammetry (CV) tests were carried out using the CHI660C electrochemical workstation in a potential range of −0.4 to 0.8 V (*vs.* Li/Li^+) at a scan rate of 1 mV s^{-1}. Electrochemical impedance spectroscopy (EIS) measurements were performed on this apparatus over a frequency range of 100 kHz to 10 mHz under AC stimulus with 10 mV of amplitude. After the electrochemical tests, the cells were disassembled by the battery removal machine (Kejing, MSK-110D).

3. Results and discussion

Fig. 1 shows the surface and cross-section SEM morphologies of a-C coatings on Si substrate, while the sputtering time is 20 min (Fig. 1a and b), 40 min (Fig. 1c and d) and 60 min (Fig. 1e and f), respectively. It can be seen that the surface is quite compact and uniform without any grain boundaries or holes. From Fig. 1b, the thickness of the a-C coating deposited for 20 min is estimated to be about 50 nm. In the same way, the thickness of the a-C coating deposited for 40 min and 60 min is about 80 nm and 110 nm, respectively.

Fig. 2 shows the surface morphologies of pure Li and Li/C electrodes before and after 50 charge/discharge cycles. Fig. 2b to Fig. 2d show the SEM images of Li/C electrodes deposited for different time spans. The island structure of amorphous carbon can be observed on the metallic Li substrate. From Fig. 2a, the surface of pure Li is not as flat as Si wafer, which can lead to the rough morphology of Li/C electrodes. There have been many reports on the morphology of the metallic Li that is electrochemically deposited in various kinds of organic electrolyte. Yamaki et al. [29] reported that there are three kinds of morphology of dendritic lithium: dendritic, granular and mossy. Fig. 2e shows the surface micrograph of pure Li electrode after 50 cycles. A granular morphology can be clearly observed. The particle-like lithium deposits are rough and loose due to the non-uniformity of SEI layer. When the lithium ions transfer between the electrodes repeatedly, the formation of dendritic morphology will occur. By contrast, the surface morphologies of Li/C electrodes in Fig. 2f to Fig. 2h are relatively blunt, indicating that no matter how long the sputtering time is, the dendritic lithium always display a mossy-like morphology.

Fig. 3 shows the C 1s and Li 1s XPS spectra of the Li/C electrode deposited for 40 min before and after 50 cycles. According to the NIST X-ray Photoelectron Spectroscopy Database, the peaks at 284.1 eV and 284.8 eV in C 1s XPS spectra can be assigned to the diamond band (D-band, sp^3 bonding) and graphite band (G-band, sp^2 bonding), respectively. In addition, the C–O bonding, C=O bonding and C–F bonding are also found at binding energy of 286.5 eV, 288.8 eV and 289.7 eV, respectively (Fig. 3a). The existence of C–O bonding and C=O bonding can be ascribed to the oxidation by O_2, while the presence of C–F bonding may result from the electrolyte vapors in glove box. Under the effect of catalytic reduction of lithium, the carbon and oxygen can react with

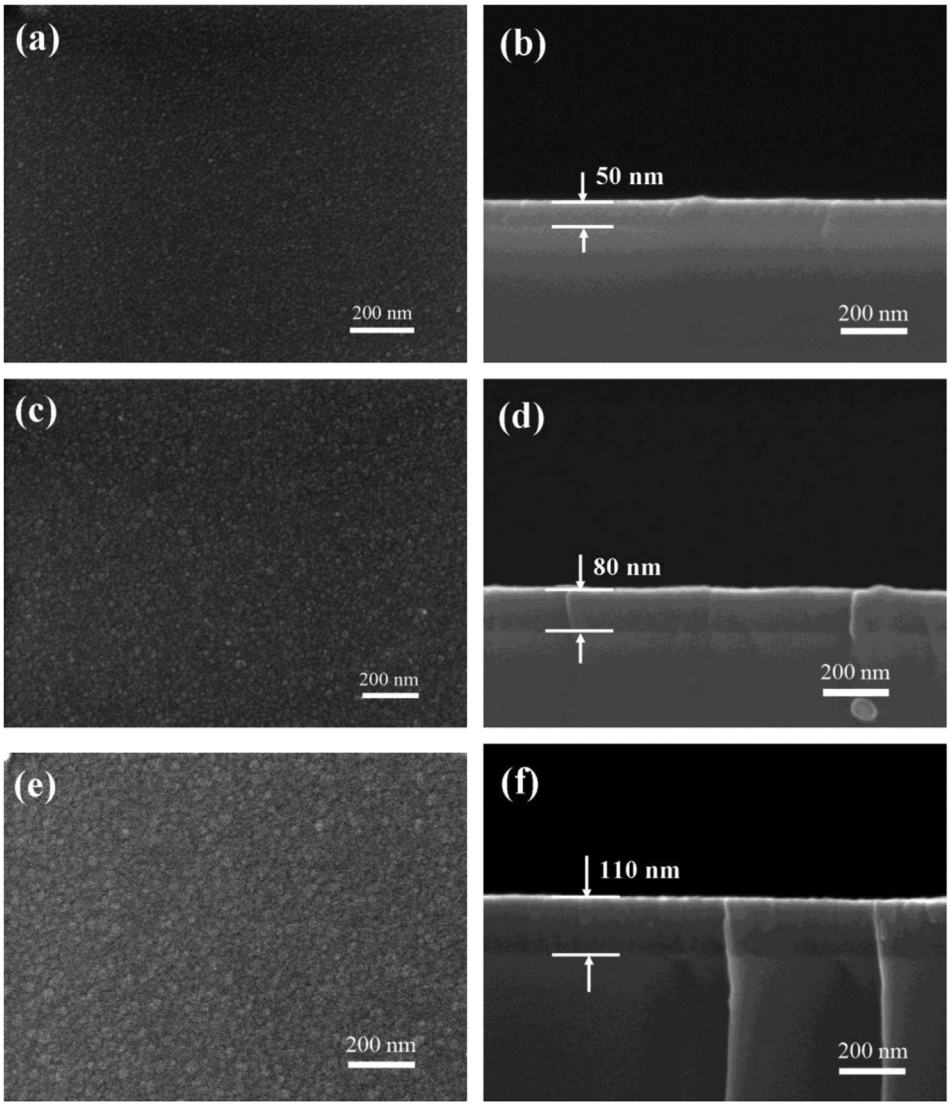

Fig. 1. Surface and cross-section SEM morphologies of carbon coatings deposited for 20 min (a and b), 40 min (c and d) and 60 min (e and f).

each other even both of these two elements are stable at room temperature (Fig. 3c). The Li 1s XPS spectra of the Li/C electrode before and after 50 cycles are shown in Fig. 3b and d, respectively. In these spectra, the peaks at 55.2 eV, 55.5 eV and 55.7 eV can be attributed to Li_2CO_3, Li_2O and LiF, respectively. The difference is there is a peak of LiOH (54.9 eV) in Fig. 3b, while an unknown peak at 58.2 eV is detected in Fig. 3d. The existence of LiOH can be ascribed to the effect of both O_2 and H_2O coming from the air. The unknown peak in Fig. 3d indicates the complicated reaction products between the metallic Li and the electrolyte during charge/discharge process. It can be expected that the a-C layer may not be that integrity after 50 cycles and the Li will react with the electrolyte. In Aurbach's research [23], a list of surface reactions between Li and electrolyte (EC–DMC/$LiPF_6$) is given, such as:

$$2EC + 2e^- + 2Li^+ \rightarrow (CH_2OCO_2Li)_2\downarrow + CH_2{=}CH_2\uparrow \quad (2)$$

$$EC + 2e^- + 2Li^+ \rightarrow LiCH_2CH_2OCO_2Li\downarrow \quad (3)$$

$$LiOH + e^- + Li^+ \rightarrow Li_2O\downarrow \quad (4)$$

$$\text{Trace } H_2O + (CH_2OCO_2Li)_2 \rightarrow Li_2CO_3 + CO_2 + (CH_2OH)_2. \quad (5)$$

$$2CO_2 + 2e^- + 2Li^+ \rightarrow Li_2CO_3\downarrow + CO\uparrow \quad (6)$$

$$LiPF_6 + H_2O \rightarrow LiF\downarrow + 2HF + PF_3O. \quad (7)$$

$$PF^{6-} + ne^- + nLi^+ \rightarrow LiF\downarrow + Li_xPF_y\downarrow \quad (8)$$

$$PF_3O + ne^- + nLi^+ \rightarrow LiF\downarrow + Li_xPOF_y\downarrow \quad (9)$$

Both solvents react to form several products, such as $ROCO_2Li$ and ROLi species. Further reduction of $ROCO_2Li$, as well as secondary reactions to these species with trace H_2O, leads to the formation of surface Li_2CO_3. The salt anion (PF^{6-}) and its related contaminants also react with Li, and hence, contribute to the complicated surface chemistry of lithium.

Fig. 4a shows the cycling efficiency of the pure Li and Li/C electrode deposited for 40 min in $LiPF_6$/EC + DMC electrolyte for 50 cycles. It is obvious that the Li/C electrode has a better cycling performance than pure Li, while the initial efficiency of two electrodes is around 80%. After 50 cycles, the coulomb efficiency of pure Li electrode reduces to 40% while the coulomb efficiency of Li/C still maintains above 80%. It is generally known that the formation of

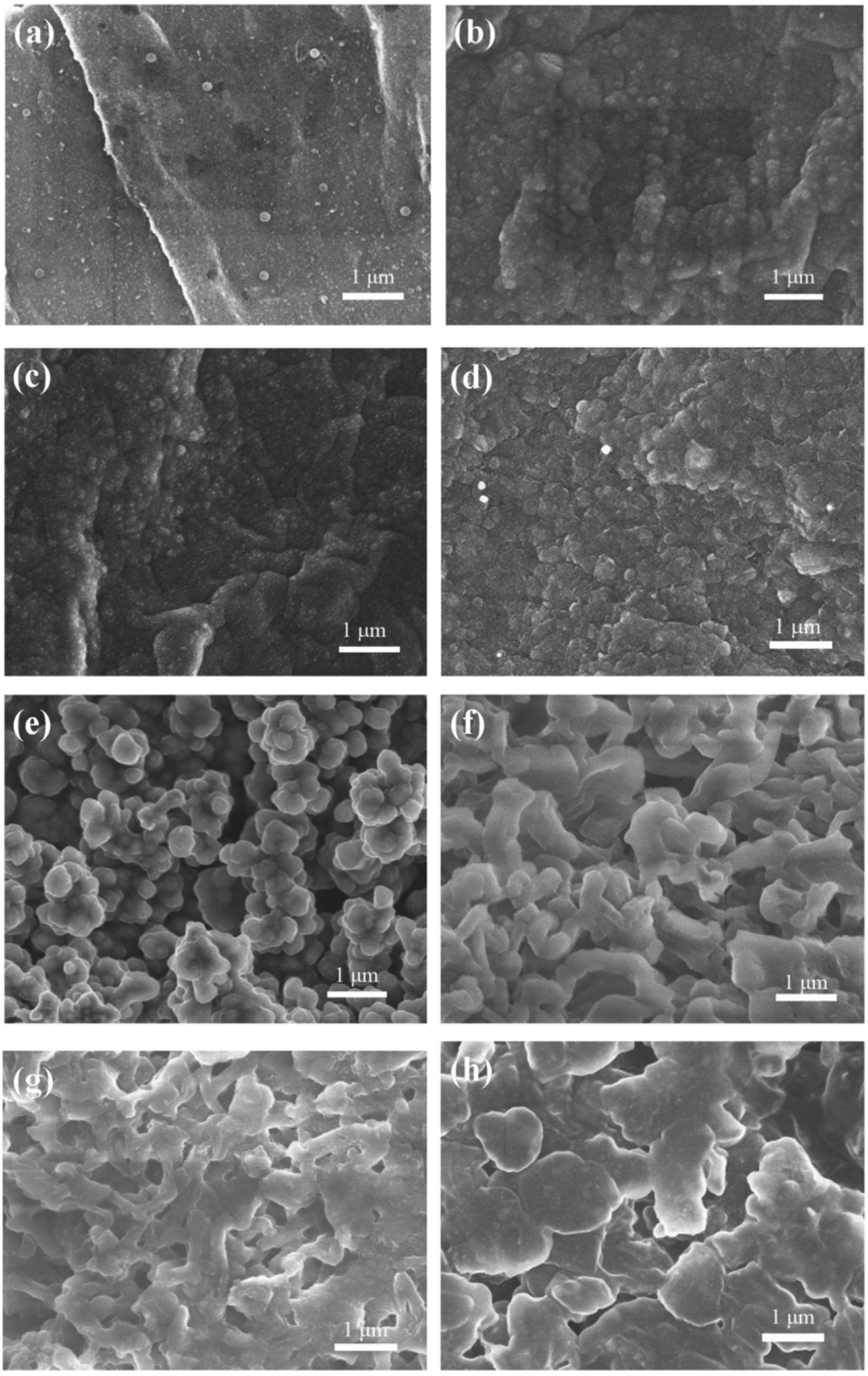

Fig. 2. Surface morphologies for pure Li and Li/C electrodes: (a) pure Li; (b) Li/C electrode deposited for 20 min; (c) Li/C electrode deposited for 40 min; (d) Li/C electrode deposited for 60 min; (e) pure Li electrode after 50 cycles; (f) Li/C deposited for 20 min after 50 cycles; (g) Li/C deposited for 40 min after 50 cycles; (h) Li/C deposited for 60 min after 50 cycles.

dendritic lithium is due to the high reactivity of metallic Li with the electrolyte, therefore it promotes a formation of non-uniform SEI layer on the surface of Li electrode. Our experiment results demonstrate that the a-C coating on Li surface can prevent the contact between the Li electrode and electrolyte, thus suppressing the formation of dendrite lithium and improving the electrochemical performance. However, the initial efficiency of both the electrodes is low. For the Li/C electrode, it is probably due to the surface oxides on Cu electrode, which may produce a Li_2O layer before Li deposited [20]. The low cycling efficiency of the pure Li electrode can be ascribed to the formation of "dead Li" on the copper electrode. As reported previously [50], there will also be

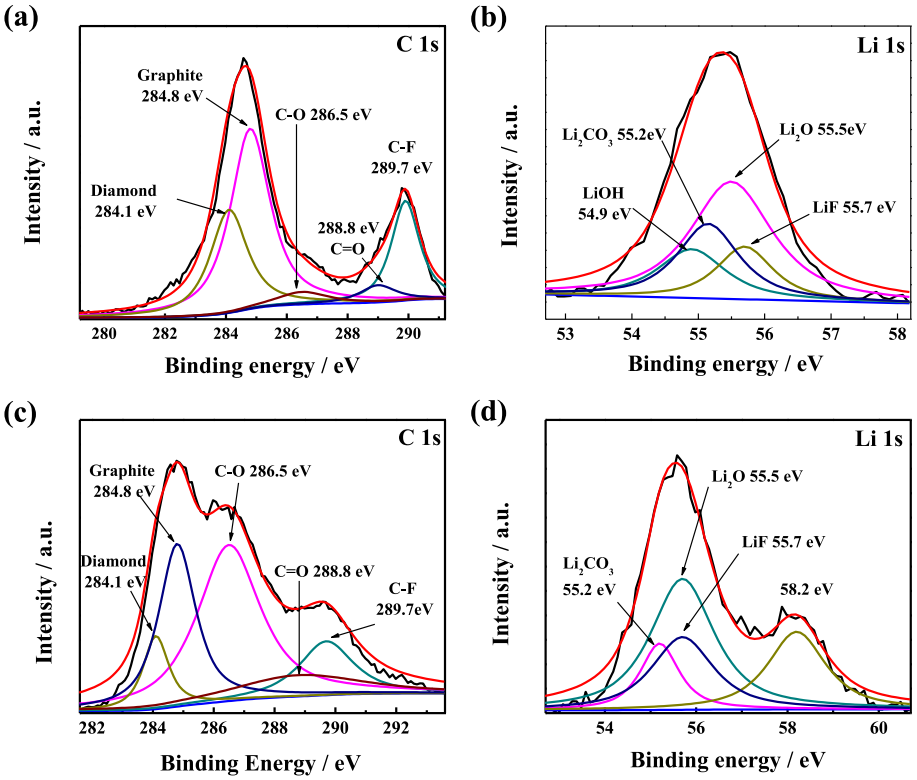

Fig. 3. C 1s and Li 1s XPS spectra of Li/C electrode deposited for 40 min: (a, b) before cycling, (c, d) after 50 cycles.

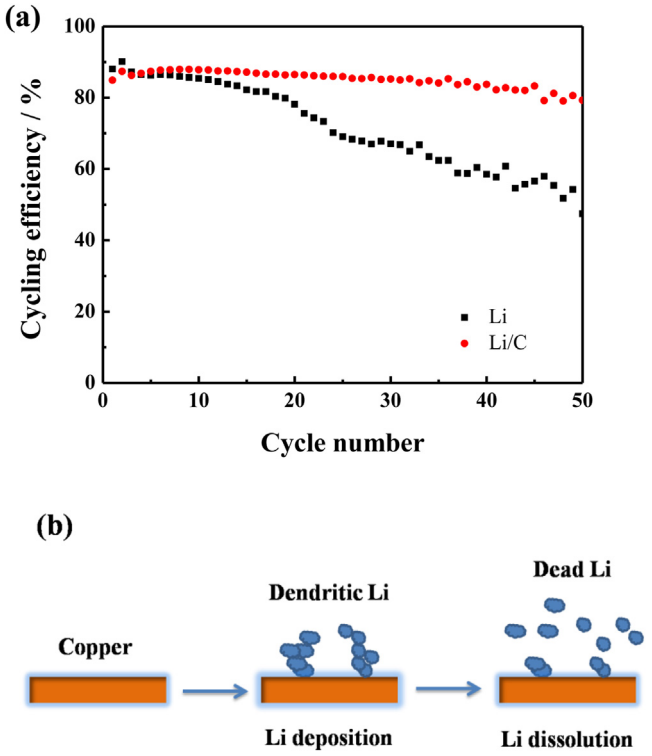

Fig. 4. (a) The cycling efficiency of pure Li and Li/C electrode deposited for 40 min, (b) the schematic diagram of the formation of "dead Li" on copper electrode.

dendritic formation when Li deposits on copper foil. During the discharge process, the uneven dissolution of the dendrites leaves Li crystals detached from the Li substrate. The isolated Li crystals become electrochemically "dead" but chemically reactive due to their high surface area, as shown in Fig. 4b.

Fig. 5 shows the Nyquist plots of the pure Li and Li/C electrodes deposited for 40 min standing at room temperature for 1 h, 1 day and 2 days. The semicircle in high frequency region represents the charge transfer resistance R_{ct} and the electrical double-layer capacitance. The straight line in low frequency region reflects the conductivity of Li^+. The smaller semicircle signifies a smaller R_{ct}, and the larger slop of the straight line gives us a better conductivity of Li^+. It can be found that, the value of R_{ct} for the pure Li electrode increases obviously along with the extension of standing time. As shown in Fig. 3, the chemical composition of Li surface is very complicated after electrochemical process, leading to the non-uniform morphology of surface film on the Li electrode. According to previous report [35], the main contribution to the resistance of pure Li electrode during cycling is from the transfer of Li^+ across the surface film. The change of semicircle radius in Fig. 5a can be ascribed to the non-uniform morphology of the Li surface. By contrast, the curve shape of Li/C electrodes shows no obvious difference as the standing time extended, indicating that the a-C coating on the Li surface can prevent the occurrence of side reaction efficiently.

CV curves of pure Li and Li/C electrodes in the potential range of −0.4 to 0.8 V are given in Fig. 6. In theory, the deposition of Li should occur when the potential sweeps to 0 V, as the redox potential of Li is around here. As a matter of fact, the electrodeposition of Li starts from −0.09 V in the negative scanning process, which represents that the deposition is an overpotential-driven nucleation/growth electrodeposition process [51]. To initiate the nucleation and subsequent growth of Li deposits, a cathodic

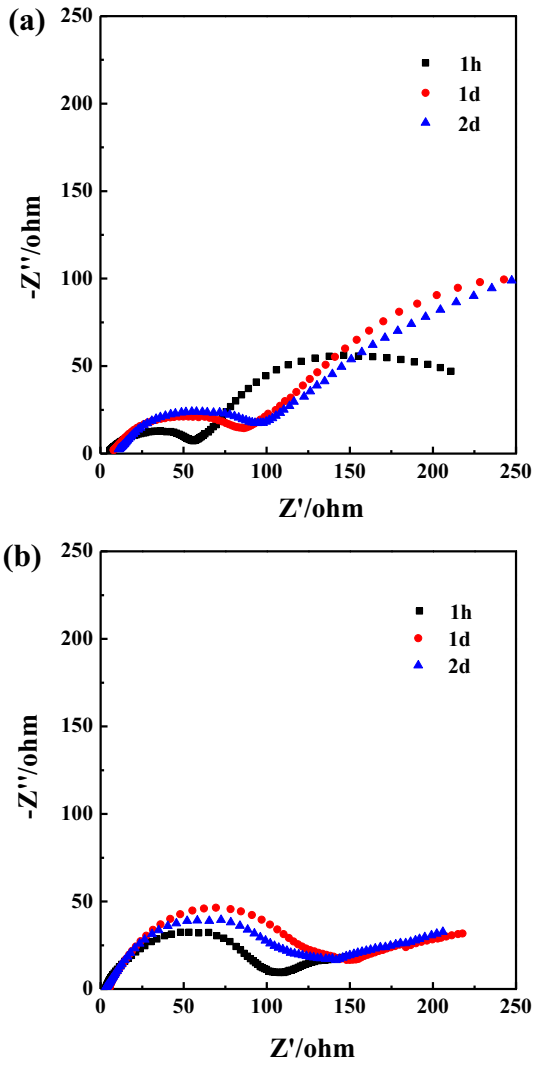

Fig. 5. Nyquist plots for (a) pure Li and (b) Li/C electrode deposited for 40 min standing for 1 h, 1 day and 2 days.

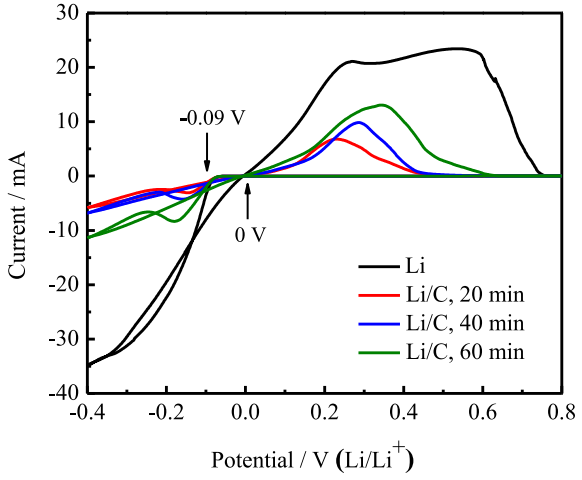

Fig. 6. CV curves of pure Li and Li/C electrodes deposited for different times.

overpotential is needed. By contrast, the pure Li electrode needs a large cathodic overpotential, indicating that a thick passive film with great resistance is formed. The larger negative potential of pure Li electrode results in less soluble reduction species precipitated on the Cu substrate [52]. The peak above 0 mA represents the dissolution process. There are two dissolution peaks for the pure Li electrode while there is only one single peak for the Li/C ones. According to previous reports [35,53], the shape of CV curves for the Li and Li_3N modified Li electrodes is similar to our results. On the CV curve of pure Li electrode, the first dissolution peak at about 0.2 V may be due to the dissolution of Li deposits because it is close to the thermodynamic redox potential of Li. The second oxidation peak at about 0.6 V can be attributed to the stripping of insoluble reduction species, which are precipitated on the Cu surface upon polarizing to more negative potential. On the CV curve of the Li/C electrodes, the single peak reflects the re-oxidation of Li deposits on the Cu substrate. On the other hand, the peak area of each Li/C electrode is much smaller than that of pure Li, indicating fewer side reactions between the Li/C electrode and electrolyte. The Li/C electrodes deposited for different times have the similar curve shapes, while the maximum deposition current and oxidation peak area change regularly. With decreasing the sputtering time, the maximum deposition current of the Li/C electrode declines, indicating that the electrode with a thinner a-C coating needs a smaller deposition current. As the maximum deposition current relates to diffusion limitation, the thin a-C coating means fast Li^+ migration in the electrode. In addition, the thicker the a-C coating is, the larger oxidation peak area the Li/C electrode shows, which represents a larger resistance when lithium ions transfer across the a-C layer. Just as shown in Fig. 2, no matter how long the sputtering time is, the dendritic lithium always displays a mossy-like morphology. Even so, the microstructure of three Li/C electrodes is obviously different from each other. With the increase of coating thickness, the mossy-like morphology becomes less obvious and the coating topography decreases. It suggests that the thick a-C coating can prevent the contact between the metallic Li and electrolyte very efficiently.

The Nyquist plots of the Li/C electrodes deposited for 20 min, 40 min and 60 min are shown in Fig. 7. All of the plots are mainly composed of a small intercept at high frequency, a semicircle at high to medium frequency and a linear part in low frequency. With increasing the thickness of a-C coating on metallic Li, the semicircle radius increases and the slope of straight line in low frequency decreases. The small semicircle radius means a low impedance of electrode, and the large slope of straight line indicates a high conductivity of Li^+. Therefore, it is concluded that a thick a-C coating will lead to a slow Li^+ transfer and increase the impedance of Li/C electrode.

Fig. 8 shows the cycling efficiency of all the Li/C electrodes for the first 100 charge/discharge cycles. It is interesting that the Li/C electrode deposited for 40 min shows the highest cycling efficiency, while the cycling performance of the Li/C one deposited for 60 min is the poorest. It is known that there is a resistance when lithium ions transfer across the a-C layer, so that the thick coating will lead to a low cycling efficiency, which can explain the low efficiency of the Li/C electrode deposited for 60 min. The excellent performance of the Li/C electrode deposited for 40 min can be attributed to the suitable coating thickness. Combined with what we have obtained in Figs. 2 and 6, the cycling performance of Li/C electrode is affected by the thickness of a-C coating from following two aspects. On one hand, the thick a-C coating can prevent the formation of dendrite much efficiently. On the other hand, the thick a-C coating will lead to a large resistance of Li^+ transfer. That is, the best electrochemical performance of Li/C electrode needs a moderate coating thickness, which can be controlled by the sputtering time.

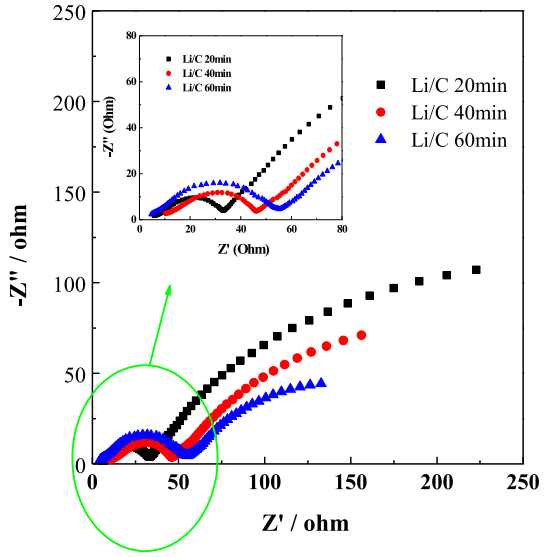

Fig. 7. Nyquist plots of Li/C electrodes deposited for 20 min, 40 min and 60 min.

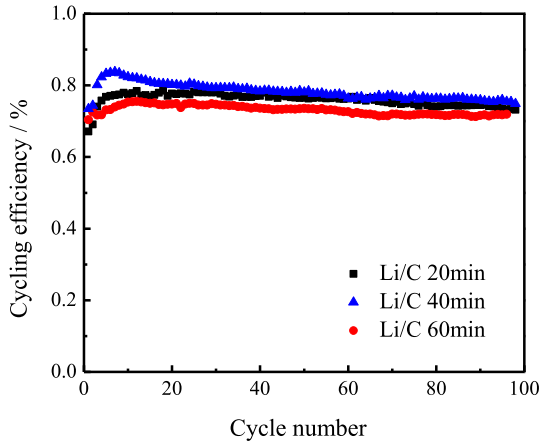

Fig. 8. Cycling efficiency for Li/C electrodes deposited for 20 min, 40 min and 60 min.

4. Conclusions

In summary, a-C coated Li electrodes were fabricated by magnetron sputtering technique. The a-C coatings on Li surface can prevent the contact between the metallic Li and electrolyte efficiently, thus suppressing the formation of dendritic lithium and improving the electrochemical performance significantly. Furthermore, the Li/C electrodes with different thicknesses of a-C coating show diverse electrochemical properties. The thickness of a-C coating affects the electrochemical performances from two aspects; the thick coating can prevent the formation of dendritic lithium very efficiently, but lead to a large resistance of Li^+ transfer. The good performance of Li/C electrode needs a moderate thickness of a-C coating, which can be controlled by the sputtering time.

Acknowledgments

This work is supported by the National Natural Science Foundation of China (50271167), the National Science and Technology Support Program (2012BAC08B08), the Program for Innovative Research Team in University of Ministry of Education of China (IRT13037) and Key Science and Technology Innovation Team of Zhejiang Province (2010R50013).

References

[1] J. Cabana, L. Monconduit, D. Larcher, M.R. Palacin, Adv. Mater. 22 (2010) E170–E192.
[2] P.I. Cowin, C.T.G. Petit, R. Lan, J.T.S. Irvine, S. Tao, Adv. Energy Mater. 1 (2011) 314–332.
[3] H.D. Oh, S.W. Lee, S.O. Kim, J.K. Lee, J. Power Sources 244 (2013) 575–580.
[4] Q.Q. Xiong, X.H. Xia, J.P. Tu, J. Chen, Y.Q. Zhang, D. Zhou, C.D. Gu, X.L. Wang, J. Power Sources 240 (2013) 344–350.
[5] W. Li, Y.X. Yin, S. Xin, W.G. Song, Y.G. Guo, Energy Environ. Sci. 5 (2012) 8007–8013.
[6] Y.Q. Zhang, X.H. Xia, X.L. Wang, Y.J. Mai, S.J. Shi, Y.Y. Tang, C.G. Gu, J.P. Tu, J. Power Sources 213 (2012) 106–111.
[7] Y. Lu, J.P. Tu, C.D. Gu, X.L. Wang, S.X. Mao, J. Mater. Chem. 21 (2011) 17988–17997.
[8] Y.Q. Zhang, X.H. Xia, X.L. Wang, Y.J. Mai, S.J. Shi, Y.Y. Tang, L. Li, J.P. Tu, Electrochem. Commun. 23 (2012) 17–20.
[9] T. Momma, M. Jeong, T. Yokoshima, H. Nara, A. Toyoda, T. Osaka, J. Power Sources 242 (2013) 527–532.
[10] Y. Lu, J.P. Tu, Q.Q. Xiong, J.Y. Xiang, Y.J. Mai, J. Zhang, Y.Q. Qiao, X.L. Wang, C.D. Gu, S.X. Mao, Adv. Funct. Mater. 22 (2012) 3927–3935.
[11] L.T. Anh, A.K. Rai, T.V. Thi, J. Gim, S. Kim, E.C. Shin, J.S. Lee, J. Kim, J. Power Sources 243 (2013) 891–898.
[12] X.Y. Zhao, J.P. Tu, Y. Lu, J.B. Cai, Y.J. Zhang, X.L. Wang, C.D. Gu, Electrochim. Acta 113 (2013) 256–262.
[13] J.C. Guo, Y.H. Xu, C.S. Wang, Nano Lett. 11 (2011) 4288–4294.
[14] S.Z. Xiong, K. Xie, Y. Diao, X.B. Hong, J. Power Sources 236 (2013) 181–187.
[15] P.G. Bruce, S.A. Freunberger, L.J. Hardwick, J.M. Tarascon, Nat. Mater. 11 (2012) 19–29.
[16] Z. Peng, S.A. Freunberger, Y. Chen, P.G. Bruce, Science 337 (2012) 563–566.
[17] Y.R. Wang, R. Ohnishi, E. Yoo, P. He, J. Kubota, K. Domen, H.S. Zhou, J. Mater. Chem. 22 (2012) 15549–15555.
[18] T. Zhang, N. Imanishi, Y. Shimonishi, A. Hirano, J. Xie, Y. Takeda, O. Yamamoto, N. Sammes, J. Electrochem. Soc. 157 (2010) A214–A218.
[19] J.L. Shui, J.S. Okasinski, P. Kenesei, H.A. Dobbs, D. Zhao, J.D. Almer, D.J. Liu, Nat. Commun. 4 (2013) 2255.
[20] F. Ding, W. Xu, G.L. Graff, J. Zhang, M.L. Sushko, X. Chen, Y. Shao, M.H. Engelhard, Z. Nie, J. Xiao, X. Liu, P.V. Sushko, J. Liu, J.G. Zhang, J. Am. Chem. Soc. 135 (2013) 4450–4456.
[21] G. Jeong, Y.U. Kim, H. Kim, Y.J. Kim, H.J. Sohn, Energy Environ. Sci. 4 (2011) 1986–2002.
[22] Z.I. Takehara, J. Power Sources 68 (1997) 82–86.
[23] D. Aurbach, E. Zinigrad, Y. Cohen, H. Teller, Solid State Ionics 148 (2002) 405–416.
[24] P. Limthongkul, Y.I. Jang, N.J. Dudney, Y.M. Chiang, J. Power Sources 119–121 (2003) 604–609.
[25] M. Rosso, C. Brissot, A. Teyssot, M. Dollé, L. Sannier, J.M. Tarascon, R. Bouchet, S. Lascaud, Electrochim. Acta 51 (2006) 5334–5340.
[26] M.H. Ryou, D.J. Lee, J.N. Lee, Y.M. Lee, J.K. Park, J.W. Choi, Adv. Energy Mater. 2 (2012) 645–650.
[27] X.Y. Wang, Y.Y. Hou, Y.S. Zhu, Y.P. Wu, R.D. Holze, Sci. Rep. 3 (2013). Art.1401.
[28] A.A. Arie, O.M. Vovk, J.O. Song, B.W. Cho, J.K. Lee, J. Electroceram. 23 (2008) 248–253.
[29] J.I. Yamaki, S.I. Tobishima, K. Hayashi, S. Keiichi, Y. Nemoto, M. Arakawa, J. Power Sources 74 (1998) 219–227.
[30] S. Shiraishi, K. Kanamura, Z.I. Takehara, J. Appl. Electrochem. 29 (1999) 867–879.
[31] M. Ishikawa, M. Morita, Y. Matsuda, J. Power Sources 68 (1997) 501–505.
[32] H. Ota, K. Shima, M. Ue, J.I. Yamaki, Electrochim. Acta 49 (2004) 565–572.
[33] Y. Takei, K. Takeno, H. Morimoto, S.I. Tobishima, J. Power Sources 228 (2013) 32–38.
[34] A.A. Arie, J.K. Lee, Diam. Relat. Mater. 20 (2011) 403–408.
[35] M.F. Wu, Z.Y. Wen, Y. Liu, X.Y. Wang, L.Z. Huang, J. Power Sources 196 (2011) 8091–8097.
[36] C.V. Falub, U. Müller, G. Thorwarth, M. Parlinska-Wojtan, C. Voisard, R. Hauert, Acta Mater. 59 (2011) 4678–4689.
[37] M. Inagaki, Carbon 50 (2012) 3247–3266.
[38] S. Wang, J.Q. Zhu, J.Z. Wang, X.B. Yin, X. Han, Thin Solid Films 519 (2011) 4906–4909.
[39] S. Zhang, X.L. Bui, Y. Fu, D.L. Butler, H. Du, Diam. Relat. Mater. 13 (2004) 867–871.
[40] F. Zhao, H.X. Li, L. Ji, Y.F. Mo, W.L. Quan, Y.J. Wang, J.M. Chen, H.D. Zhou, Thin Solid Films 519 (2011) 2043–2048.
[41] J. Díaz, G. Paolicelli, S. Ferrer, F. Comin, Phys. Rev. B 54 (1996) 8064–8069.
[42] P. Mérel, M. Tabbal, M. Chaker, S. Moisa, J. Margot, Appl. Surf. Sci. 136 (1998) 105–110.
[43] J. Schwan, S. Ulrich, V. Batori, H. Ehrhardt, S.R.P. Silva, J. Appl. Phys. 80 (1996) 440–447.
[44] J.B. Cai, X.L. Wang, W.Q. Bai, X.Y. Zhao, T.Q. Wang, J.P. Tu, Appl. Surf. Sci. 279 (2013) 450–457.

[45] K.E. Cooke, J. Hamsphire, W. Southall, D.G. Teer, Surf. Coat. Technol. 177–178 (2004) 789–794.
[46] P.J. Kelly, R. Hall, J. O'Brien, J.W. Bradley, P. Henderson, G. Roche, R.D. Arnell, J. Vac. Sci. Technol. A 19 (2001) 2856–2865.
[47] I. Petrov, P.B. Barna, L. Hultman, J.E. Greene, J. Vac. Sci. Technol. A 21 (2003) S117–S128.
[48] V.N. Popok, Mater. Sci. Eng. R 72 (2011) 137–157.
[49] M. Rahamathunnisa, D.C. Cameron, Surf. Coat. Technol. 204 (2010) 3131–3134.
[50] K. Xu, Chem. Rev. 104 (2004) 4303–4418.
[51] R.J. Nichols, W. Beckmann, H. Meyer, N. Batina, D.M. Kolb, J. Electroanal. Chem. 330 (1992) 381–394.
[52] D. Aurbach, Y. Cohen, J. Electrochem. Soc. 143 (1996) 3525–3532.
[53] R. Wibowo, S.E. Ward Jones, R.G. Compton, J. Phys. Chem. B 113 (2009) 12293–12298.